CHEMISTRY OF MATERIALS

pubs.acs.org/cm

Article

Sodium Selenotetrelates with Isolated $TtSe_4$-Tetrahedra (*Tt* = Si, Ge, Sn): Synthesis, Crystal Structures, Thermal Behavior, DFT Modeling, and Na Ion Conductivities

Published as part of Chemistry of Materials virtual special issue "In Memory of Prof. Francis DiSalvo".

Franziska Kamm, Florian Pielnhofer,* and Arno Pfitzner*

Cite This: *Chem. Mater.* 2024, 36, 5643−5650

Read Online

ACCESS | Metrics & More | Article Recommendations | Supporting Information

ABSTRACT: Selenotetrelate compounds Na_4TtSe_4 (*Tt* = Si, Ge, Sn) were synthesized by solid-state reactions. A new modification of Na_4SiSe_4 (Na_4SiSe_4-*cP*72), which crystallizes in the cubic space group $P\bar{4}3n$ (no. 218) with a = 12.130(1) Å and V = 1784.453(5) Å^3, and a new modification of Na_4SnSe_4 (Na_4SnSe_4-*tI*216), which crystallizes in the tetragonal space group $I4_1/acd$ (no. 142) with a = 14.4053(4) Å, c = 28.5751(8) Å and V = 5929.7(3) Å^3, were discovered. All of the title compounds exhibit moderate to good sodium ion conductivities, as revealed by electrochemical impedance spectroscopy. The formation reaction of Na_4SiSe_4 was further investigated by high-temperature X-ray powder diffraction of the ball-milled reaction mixture. Density functional-based quantum chemical calculations were performed to compare the different modifications of Na_4SiSe_4 and Na_4SnSe_4 energetically. Further modifications of Na_4SiSe_4 and Na_4GeSe_4 seem plausible, as revealed by density functional theory modeling. The stability of the hypothetic modifications was examined by phonon dispersion calculations.

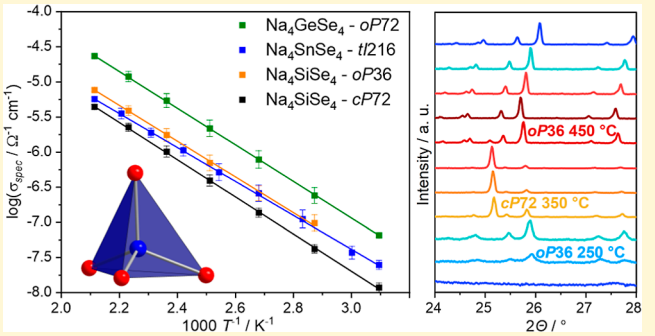

INTRODUCTION

All-solid-state-batteries (ASSBs) became promising options for battery systems.[1,2] One of the key components in ASSBs is the solid electrolyte, which must exhibit high ionic conductivities. After concentrating on lithium-based systems for a long time, research focused on solid sodium ion conductors recently.[3−5] In particular, for stationary applications, sodium-based batteries are a valuable alternative to lithium-based systems. Due to the higher abundance of sodium, the costs for battery systems can be significantly lowered.

Some of the highest sodium ion conductivities were found in sulfides such as the thiophosphate Na_3PS_4.[6,7] By substitution of S with Se, the ionic conductivity could be further increased.[8−10] Furthermore, the charge carrier density and therefore also the ionic conductivity can be increased by the incorporation of tetrels, for example, in $Na_{10}SnP_2S_{12}$.[11−13] Despite that, ternary sodium selenotetrelates are less investigated regarding their sodium ion conductivity.

A variety of structure types including different anions exist among ternary alkali metal, tetrel (*Tt* = Si, Ge, Sn) and chalcogenide (*Q* = S, Se, Te) containing materials. Most of them consist of TtQ_4 tetrahedra, which are connected in different ways. This includes isolated TtQ_4 tetrahedra,[14−20] dimers Tt_2Q_7 from corner-sharing tetrahedra,[21] infinite chains Tt_2Q_6 of tetrahedra sharing two corners,[22] or layers of corner-sharing $GeSe_4$-tetrahedra.[23] In the perselenodisilicate $Na_6Si_2Se_8$, two $SiSe_4$ tetrahedra are connected by a Se−Se bond to form $Si_2Se_8^{6-}$ units.[24] Adamantan-analogous units are found in $Na_4Si_4Se_{10}$[22] and $Na_4Ge_4Se_{10}$.[25] Even *Tt*−*Tt* bonds are present in hypoditetrelates to form ethane molecule analogous anions.[26−28] Edge-sharing $SiSe_4$ tetrahedra dimers are exclusively observed in $Na_4Si_2Se_6$-*tP*24.[29] Especially the physical and chemical characterization of sodium selenotetrelates is very scarce in the literature. To date, the focus has been mostly set on crystal growth and determination of crystal structures. Minor interest arose for the phase pure synthesis and investigation of physical properties, e.g., ion conductivity, when these compounds were first discovered. In contrast to the selenides, the sulfides Na_4SiS_4,[30] Na_4GeS_4,[31] and Na_4SnS_4[32,33] were characterized regarding their chemical and physical properties. All sodium thiotetrelates show sodium ion conductivity. It can therefore be assumed that also sodium selenotetrelates show sodium ion conductivity and should be

Received: March 6, 2024
Revised: April 25, 2024
Accepted: April 25, 2024
Published: May 16, 2024

examined systematically. Two selenide compounds were already checked for the sodium ion mobility. Impedance spectroscopy measurements reveal moderate to good ionic conductivities for $Na_4Si_2Se_6$-*oP*48[29] (1.4×10^{-8} S cm^{-1} at 50 °C) and Na_4SnSe_4-*tP*18[32] (1.13×10^{-8} S cm^{-1} at 20 °C).

Herein, we focus on sodium selenotetrelates with isolated $TtSe_4$ tetrahedra (*Tt* = Si, Ge, and Sn). Many alkali metal compounds containing this structural motif are already known (Table 1). Most of the selenotetrelates described in the literature were synthesized by classical high-temperature solid-state routes. Other methods, such as the use of ball mills, open the possibility to synthesize new compounds in the already well-established system. Besides the determination of sodium ion conductivity in already known sodium selenotetrelates Na_4TtSe_4, new modifications of Na_4SiSe_4 and Na_4SnSe_4 were discovered. The two-step synthesis procedure consisting of ball milling, followed by annealing, was examined for Na_4SiSe_4. Starting from the ball-milled reaction mixture, the formation of the two modifications of Na_4SiSe_4 can be followed with in situ high-temperature X-ray powder diffraction. The stability of the new modifications was further studied by density functional theory (DFT) modeling, including yet unknown hypothetical modifications. Ionic conductivities were determined for all of the title compounds.

Table 1. Compounds and Structure Types of Alkali Selenotetrelates

structure type	examples	space group
Li_4GeS_4[34]	Li_4GeSe_4-*oP*36,[15] Li_4SnSe_4-*oP*36[14a]	*Pnma* (no. 62)
Na_4GeSe_4[16]	Na_4GeSe_4-*oP*72	*Pnma* (no. 62)
Na_4SnS_4[35]	Na_4SnSe_4-*tP*18[17]	$P\bar{4}2_1c$ (no. 114)
K_4SnSe_4[17]	Na_4SiSe_4-*oP*36,[18] K_4SnSe_4-*oP*36	*Pnma* (no. 62)
Ba_4SiAs_4[19]	K_4GeSe_4-*cP*72,[36] Cs_4SiSe_4-*cP*72[20]	$P\bar{4}3n$ (no. 218)

[a]Both compounds have the same building principle and the same space group but show minor differences in the Li substructure.

EXPERIMENTAL SECTION

Synthesis. All preparations and sample treatments were performed under an Ar atmosphere.

The title compounds were synthesized from the elements. Sodium (Sigma-Aldrich, 99.8%), silicon (silicon wafer, siltronic), tin (ChemPur, 99+%), and selenium (ChemPur, 99.99%) were used as received. Germanium (ChemPur, 99.99%) was purified in H_2 atmosphere at 600 °C and stored in the Ar atmosphere. Syntheses were performed in a FRITSCH pulverisette 7 premium line ball mill with 25 mL zirconia grinding bowls and 10 zirconia grinding balls with a diameter of 10 mm. In each case, 0.3 g of the ball-milled mixture was transferred to silica ampules which were subsequently evacuated, flame-sealed, and transferred to tube furnaces. In case the reaction temperature was higher than 600 °C, silica ampules with a graphite coating from pyrolyzed acetone were used to prevent reactions with the glass.

Na_4SiSe_4-*oP*36 and Na_4SiSe_4-*cP*72 were synthesized by ball milling Na, Si, and Se with a molar ratio of 4:1:4 in 12 milling cycles at a top speed of 600 rpm for 3 min each. For Na_4SiSe_4-*cP*72, the mixture was then heated to 375 °C with a heating rate of 1 °C min^{-1}. After 10 days, the ampule was quenched in air. Small amounts of Na_2Se_2 (3.8% according to Rietveld refinements) were detected as side phase. To synthesize Na_4SiSe_4-*oP*36, the mixture was heated to 500 °C for 3 days. Both heating and cooling rates were set to 1 °C min^{-1}.

Na_4GeSe_4-*oP*72 was synthesized by ball milling Na, Ge, and Se with a molar ratio of 4:1:4. Twelve milling cycles at a top speed of 600 rpm were performed. The mixture was then heated to 400 °C for 7 days. Both heating and cooling rates were set to 1 °C min^{-1}.

Na_4SnSe_4-*tI*216 was synthesized by ball milling Na, Sn, and Se with a molar ratio of 4.1:1:4. Three milling cycles with a top speed of 300 rpm followed by 25 milling cycles at 400 rpm were performed. The mixture was then heated to 800 °C with a heating rate of 0.5 °C min^{-1} and kept at this temperature for 1 h. After cooling down slowly within 1 day, orange crystals were observed.

X-ray Powder Diffraction. Finely ground samples were filled in quartz capillaries (⌀ = 0.3 mm) that were subsequently flame-sealed. The capillaries were mounted on a STOE STADI P diffractometer (Stoe & Cie) equipped with a Mythen 1 K detector and measured using Cu$K\alpha_1$ radiation (λ = 1.5406 Å). The high-temperature diffraction experiment was performed in a graphite furnace, which was mounted on the diffractometer. For raw data handling, the WinXPow[37] software package (Stoe & Cie) was used. Le Bail refinements, structure solution, and Rietveld refinements were done with Jana2006[38] and the implemented Superflip[39] algorithm.

Single-Crystal X-ray Diffraction. The single-crystal diffraction experiment was performed at 296 K on a Rigaku SuperNova diffractometer with an AtlasS2 detector using Mo$K\alpha$ radiation (λ = 0.71073 Å). For cell determination, data reduction, and absorption correction, the CrysAlis Pro software[40] was used. The structure was solved using the Superflip[39] algorithm which is implemented in Jana2006.[38] Structure refinement was also performed with Jana2006.

Differential Thermal Analysis. For differential thermal analysis (DTA) measurements, a SETARAM TG-DTA 92.16.18 was used. Samples were transferred into quartz tubes (⌀ = 2 mm) which were evacuated and flame-sealed. Thermal properties were investigated up to 800 °C.

Impedance Spectroscopy. Electrochemical impedance spectroscopy (EIS) was performed with a Zahner Zennium impedance analyzer coupled to a homemade furnace. The complete setup was installed in a glovebox under an Ar atmosphere to prevent reactions of the samples with air or moisture during the measurements. Because of this setup, no measurements below 50 °C were possible. Powder samples were cold-pressed and contacted with gold electrodes. Pellets had a density of 96% (Na_4SiSe_4-*oP*36), 86% (Na_4SiSe_4-*cP*72), 96% (Na_4GeSe_4), and 90% (Na_4SnSe_4-*tI*216). In each case, two temperature cycles in the frequency range from 1 MHz to 100 mHz were recorded. For the different compounds, different temperature ranges and temperature steps were used. Na_4SiSe_4-*oP*36, Na_4SiSe_4-*cP*72, and Na_4GeSe_4 were analyzed in the temperature range from 50 to 200 °C in steps of 25° and Na_4SnSe_4-*tI*216 from 50 to 200 °C in steps of 20 °C. The excitation voltage was set to 50 mV in each case. Ionic conductivities were determined from the second heating and cooling cycles since the contact between pellets and electrodes is much better. For data processing and fitting, the *Zahner Analysis* software[41] was used. Nyquist plots were fitted by different equivalent circuits (see Figure S14). The so-determined resistance *R* was corrected by including the density of the pellet to calculate the specific conductivity σ_{spec}. Activation energies E_A were determined from the slopes in the Arrhenius plots. For Na_4SiSe_4-*oP*36, the evaluation of the ionic conductivity at 50 °C was not possible due to the bad quality of the measured data. After the measurements, all samples were checked for decomposition or phase transitions by X-ray powder diffraction. Apart from the expected peak broadening, all samples were identical to the starting material, which is especially important for the cubic modification.

DFT Modeling. All quantum chemical calculations were performed using the CRYSTAL17 code.[42,43] Basis sets (Na,[44] Si,[45] Ge,[46] Sn,[47] and Se[48]) were taken from the literature. The outer shells of all of the basis sets were additionally adjusted to minimize the calculated energy. Full structure optimizations within the given space groups were performed with the hybrid HSE06[49,50] using a *k* mesh sampling of 6 × 6 × 6. The convergence criterion for the energy was set to 10×10^{-8} au. Geometries were optimized using experimentally determined structure data as starting point. For calculation of electronic energy *E* vs volume per formula unit *V* curves, constant volume optimizations were performed using the GGA functional PBE.[51] Data was fitted with the Birch–Murnaghan equation of state.[52−54] For electronic band structure calculations, the hybrid

https://doi.org/10.1021/acs.chemmater.4c00670
Chem. Mater. 2024, 36, 5643−5650

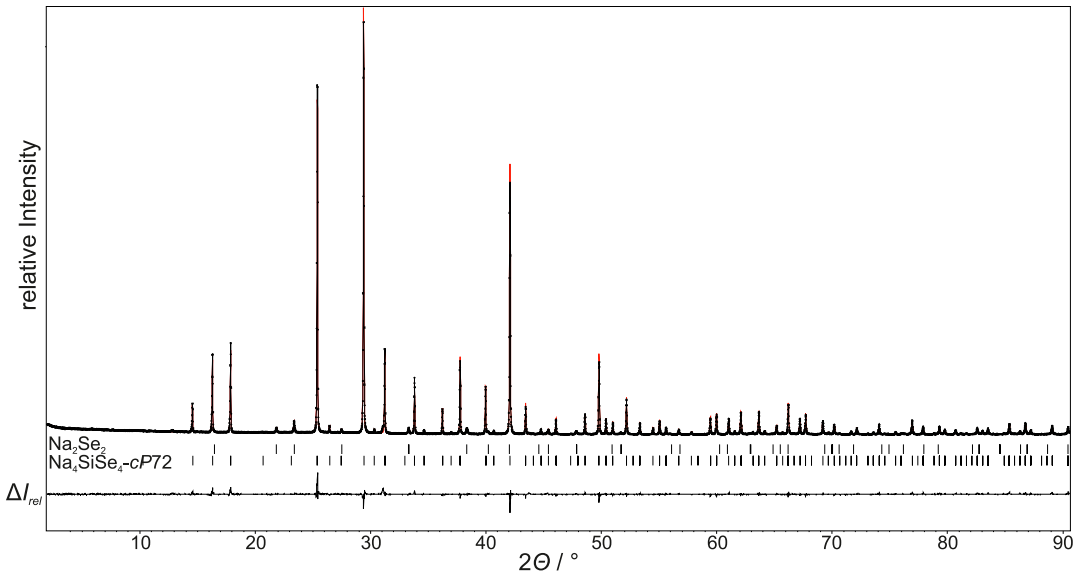

Figure 1. X-ray powder diffraction pattern of Na_4SiSe_4-*cP*72 with difference plot from Rietveld refinement. The side phase was determined to be Na_2Se_2[58] (3.8%).

HSE06 was used. *k* paths were determined using the SeeK-path online tool.[55] Phonon frequencies including LO-TO splitting were calculated, as implemented in CRYSTAL17.[56,57] Because of the high computational effort, calculations were performed on the PBE level with a 2 × 2 × 2 super cell and a *k* mesh sampling of 4 × 4 × 4. To increase accuracy for phonon frequency calculation, the SCF convergence criterion was set to 10×10^{-10} au.

RESULTS AND DISCUSSION

Crystal Structure of Na_4SiSe_4-*cP*72. The new modification Na_4SiSe_4-*cP*72 crystallizes in the cubic space group $P\bar{4}3n$ (no. 218) with $a = 12.1295(1)$ Å and $V = 1784.543(5)$ Å^3; $Z = 8$. The crystal structure was determined by powder X-ray diffraction via Superflip and the Rietveld method (Figure 1). Further crystallographic data and structure determination details can be found in Table 2 and in Supporting Information (Tables S1 and S2).

The main structural features are the isolated $SiSe_4$ tetrahedra, which are also found in the second modification Na_4SiSe_4-*oP*36.[18] The unit cell with all isolated $SiSe_4$ tetrahedra is shown in Figure 2. Na_4SiSe_4-*cP*72 adopts the Ba_4SiAs_4 structure type,[19] which is described in detail by Eisenmann et al. The crystal structure can be derived from the NaCl structure type, with Se^{2-} forming a distorted face-centered cubic lattice where Na^+ occupies all octahedral voids. Additionally, Si^{4+} occupies $\frac{1}{8}$ of all tetrahedral voids in an ordered manner.

There are two crystallographically different $SiSe_4$ tetrahedra with distances *d*(Si−Se) of 2.248(2) Å for Si1 and 2.2543(9) Å for Si2. Angles deviate only slightly from ideal tetrahedra angles (109.47(6)° for Si1; 107.27(4)° and 113.97(3)° for Si2). Na1 and Na2 are both coordinated octahedrally with distances *d*(Na−Se) varying from 2.933(4) to 3.245(4) Å. All interatomic distances are in the expected range. A comparison of distances and angles in both modifications of Na_4SiSe_4 is given in Table S3. Crystal structures of both modifications can be derived from space group $Fm\bar{3}m$ (no. 225), but there is no direct group−subgroup relation.

Crystal Structure of Na_4SnSe_4-*tI*216. The new modification Na_4SnSe_4-*tI*216 crystallizes in the tetragonal space group $I4_1/acd$ (no. 142) with lattice parameters $a = 14.4098(4)$ Å, $c = 28.5851(8)$ Å and $V = 5935.5(3)$ Å^3 with $Z = 24$. Further crystallographic data and structure determination details can be found in Table 2 and Supporting Information (Tables S6 and S7).

The structure type is already known from Na_4SnTe_4-*tI*216.[59] As a detailed structure discussion for Na_4SnS_4, which crystallizes in the same structure type, is already given by Hartmann et al.,[33] only the primary features will be mentioned in the following. The main structural motifs are isolated $SnSe_4$ tetrahedra (Figure 3). There are two distinct Sn positions with a tetrahedral coordination with distances *d*(Sn−Se) from 2.5106(2) to 2.5286(2) Å. Na1, Na2, and Na3 are coordinated octahedrally with distances *d*(Na−Se) varying from 2.8319(2) to 3.3821(8) Å. Na4 is surrounded tetrahedrally with distances

Table 2. Crystallographic Data and Structure Determination Details for Na_4TtSe_4 with *Tt* = Si, Sn[a]

compound	Na_4SiSe_4-*cP*72	Na_4SnSe_4-*tI*216
space group	$P\bar{4}3n$ (no. 218)	$I4_1/acd$ (no. 142)
formula weight/g mol^{-1}	435.9	526.5
shape, color	powder, brown	block, yellow
T/K	296	296
a/Å	12.1295(1)	14.4053(4)
c/Å		28.5751(8)
V/Å^3	1784.543(5)	5929.7(3)
Z	8	24
radiation	Cu Kα_1 (λ = 1.5406 Å)	MoKα (λ = 0.71073 Å)
R_{int}		0.0295
profile *R* indexes	R_P = 0.0490, R_{wp}= 0.0681, R_{exp} = 0.0430	
goodness of fit	1.58	1.22
final *R* indexes [$I \geq 3\sigma(I)$]	R_1 = 0.0376, wR_1 = 0.0452	R_1 = 0.0187, wR_1 = 0.0422
final *R* indexes [all data]	R_2 = 0.0398, wR_2 = 0.0456	R_2 = 0.0274, wR_2 = 0.0451
$\Delta\rho_{min}$, $\Delta\rho_{max}$/eÅ^{-3}	−0.79, 0.85	−1.29, 0.75

[a]Note that Na_4SiSe_4-*cP*72 was determined from powder data, and Na_4SnSe_4-*tI*216 from a single crystal.

https://doi.org/10.1021/acs.chemmater.4c00670
Chem. Mater. 2024, 36, 5643−5650

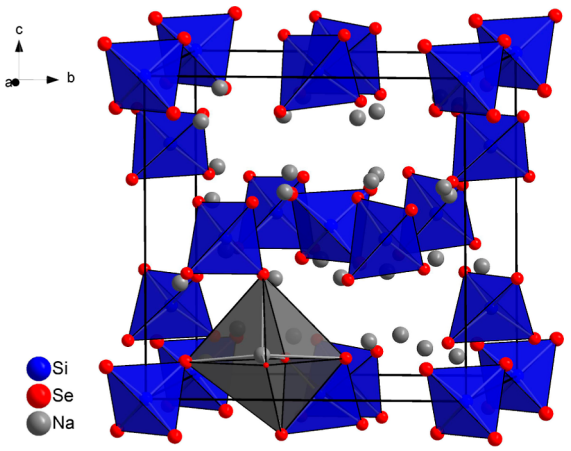

Figure 2. Unit cell of Na_4SiSe_4-*cP*72 with Na and Si coordination polyhedra.

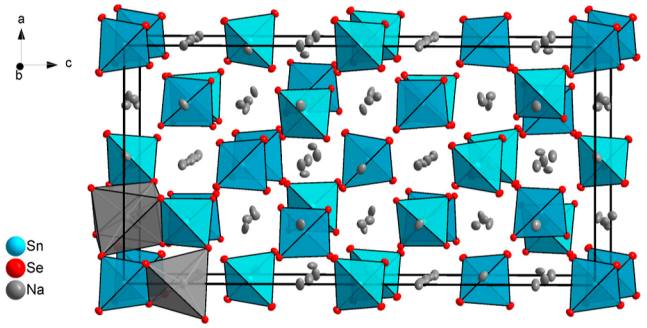

Figure 3. Unit cell of Na_4SnSe_4-*tI*216 with isolated $SnSe_4$ tetrahedra and Na coordination polyhedra.

d(Na4−Se) of 2.9449(7) and 2.990(1) Å. Na5 has a distorted trigonal bipyramidal coordination with distances *d*(Na5−Se) varying from 2.9625(9) to 3.358(1) Å. A further Se at a distance *d*(Na5−Se) of 3.9255(9) Å completes the coordination environment to a strongly distorted octahedron. Na−Se polyhedra form a 3D network with nearly linear and zigzag chains in the *c*-direction and in the *ab*-plane. All interatomic distances are in the expected range. A comparison of distances and angles in both modifications of Na_4SnSe_4 is given in Table S8.

Formation, Stability, and Electronic Structures of Na_4TtSe_4. *Na_4SiSe_4.* To further study the polymorphism, high-temperature X-ray powder diffraction was performed starting from the ball-milled reaction mixture. Thereby, the formation process of both modifications from binary Na_2Se_2 and Si can be followed by slowly heating the sample (Figure 4). Below 200 °C, only Na_2Se_2 (101, 2Θ = 23.4°) and Si (111, 2Θ = 28.5°) are present. With increasing temperature, at 250 °C, new reflections occur which can be assigned to Na_4SiSe_4-*oP*36 (102, 2Θ = 25.8°). At 350 °C, the formation of Na_4SiSe_4-*cP*72 (222, 2Θ = 25.2°; 004, 2Θ = 29.1°) can be observed. The cubic modification is stable only in a small temperature range (350 to 400 °C). At higher temperature, only Na_4SiSe_4-*oP*36 is observed. Even upon cooling to room temperature, the transformation to Na_4SiSe_4-*cP*72 cannot be detected again. Because of the reaction of Na with the quartz capillary, X-ray powder diffraction measurements at temperatures higher than 500 °C were not possible. A comparison of the total electronic energy shows that Na_4SiSe_4-*cP*72 is more stable by 8.5 kJ mol^{-1} (Figure 5) relative to Na_4SiSe_4-*oP*36. According to Ostwald's rule, the metastable modification, Na_4SiSe_4-*oP*36, should crystallize before the stable modification. This was confirmed by high-temperature X-ray powder diffraction. It is remarkable that the cubic modification disappears at temperatures higher than 400 °C. Probably different thermodynamic and kinetic effects play a role here. Nevertheless, the high-temperature powder X-ray diffraction experiment helps to determine the reaction conditions for the synthesis of new modifications even if they are stable only in a small temperature range. In accordance with the measurement, samples of Na_4SiSe_4-*cP*72 containing less than 5% of Na_2Se_2 as a side phase can be obtained by heating up to 375 °C for 10 days.

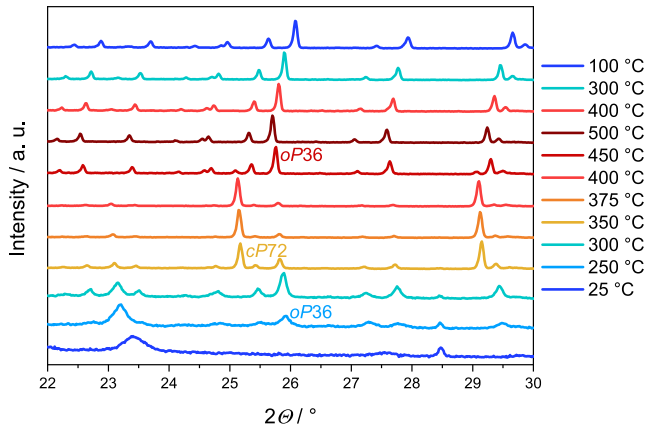

Figure 4. X-ray powder diffraction patterns of the ball-milled reaction mixture of "Na_4SiSe_4". Up to 200 °C, Na_2Se_2 and Si are present. With further heating, Na_4SiSe_4-*oP*36 forms. At 350 to 400 °C, Na_4SiSe_4-*cP*72 is present.

To examine also higher temperatures, DTA of the ball-milled reaction mixture was performed (heating/cooling rate 5 °C min^{-1}) (Figure S6). Formation peaks of Na_4SiSe_4-*cP*72 and Na_4SiSe_4-*oP*36, which are expected at approximately 300 and 400 °C, are not visible. We assume that the formation reaction of the products is too slow in a relatively wide temperature range to be detectable via DTA. Peaks at 553 °C in the first cooling cycle and 548 °C in the second cooling cycle can be assigned to the crystallization temperature of Na_4SiSe_4-*oP*36. Samples of the ball-milled reaction mixture as well as Na_4SiSe_4-*oP*36 were heated to 800 °C, subsequently cooled to 570 and 500 °C (5 °C min^{-1}), and quenched in water. All of these synthesis attempts resulted in only Na_4SiSe_4-*oP*36, so the DTA peaks probably stem from a recrystallization of Na_4SiSe_4-*oP*36. Quenching in water from 700 °C results in an amorphous product. DTA measurements of Na_4SiSe_4-*oP*36 and Na_4SiSe_4-*cP*72 are shown in the Supporting Information (Figures S7 and S8).

As mentioned before, equation of state calculations show that Na_4SiSe_4-*cP*72 is more stable by 8.5 kJ mol^{-1} relative to Na_4SiSe_4-*oP*36 (Figure 5a). DFT modeling of Na_4SiSe_4 in different hypothetical structure types, which are known from Na_4GeSe_4 and Na_4SnSe_4, reveals only small energy differences. Hypothetical Na_4SiSe_4 in the Na_4SnS_4 structure type (Na_4SiSe_4-*tP*18, Figure 5d) is 1.9 kJ mol^{-1} lower in energy than Na_4SiSe_4-*cP*72. Hypothetical Na_4SiSe_4-*tI*216 (Na_4SnTe_4-*tI*216 structure type) and Na_4SiSe_4-*oP*72 (Na_4GeSe_4 structure type) are 3.0 and 8.1 kJ mol^{-1} higher in energy. Na_4SiSe_4-*oP*36, which was the first discovered modification, is 10.0 kJ mol^{-1}

https://doi.org/10.1021/acs.chemmater.4c00670
Chem. Mater. 2024, 36, 5643−5650

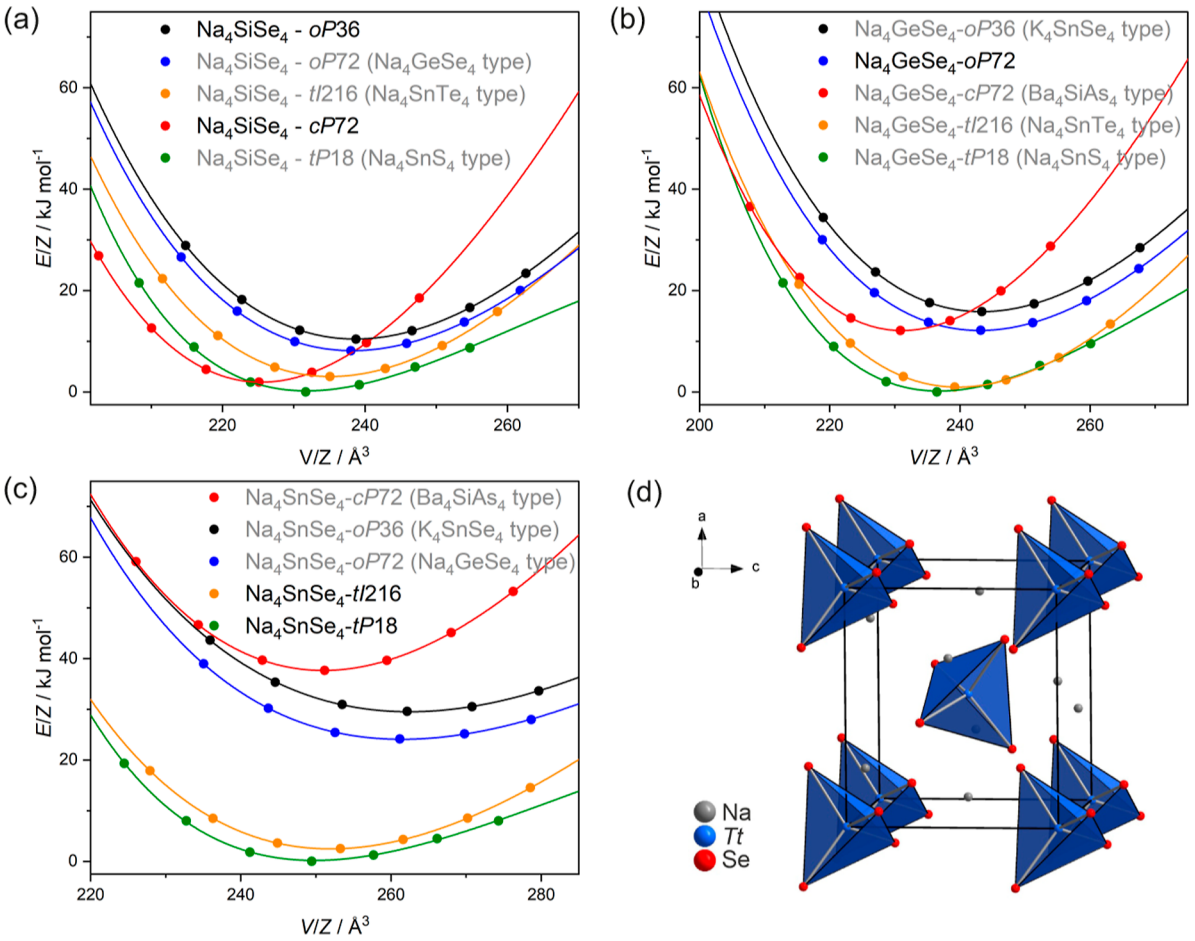

Figure 5. Calculated E vs V curves for different (hypothetic) modifications of (a) Na_4SiSe_4, (b) Na_4GeSe_4, and (c) Na_4SnSe_4. Hypothetical compounds are written in gray, whereas the experimentally detected modifications are written in black. According to the E vs V plots, no pressure-dependent phase transition of the investigated compounds is expected. (d) Unit cell of the Na_4TtSe_4-*tP*18 structure with isolated $TtSe_4$-tetrahedra.

higher in energy relative to Na_4SiSe_4-*tP*18. As all considered structure types are relatively close in energy, the existence of further modifications of Na_4SiSe_4 seems plausible.

To check for the stability of the most stable hypothetical modification of Na_4SiSe_4, the *tP*18 modification was additionally probed by calculation of phonon frequencies (Figure S13). No physically relevant imaginary frequencies were obtained, thus indicating a dynamically stable structure.

Na_4GeSe_4. Even though no further modification of Na_4GeSe_4 except the already known one Na_4GeSe_4-*oP*72 could be experimentally detected, DFT modeling of Na_4GeSe_4 in different possible structure types was performed. Calculated $E-V$-curves (Figure 5b) show that there are three possible modifications that are lower in energy than the experimentally observed one. Na_4GeSe_4-*tP*18 (Na_4SnS_4 structure type) and Na_4GeSe_4-*tI*216 (Na_4SnTe_4 structure type) are 12.2 and 11.2 kJ mol^{-1} lower in energy with respect to Na_4GeSe_4-*oP*72. Na_4GeSe_4-*cP*72 (Ba_4SiAs_4 structure type) is 0.03 kJ mol^{-1} lower in energy. Phonon frequencies were calculated for Na_4GeSe_4 in the Na_4SnS_4 structure type (Figure S13). As no physically relevant imaginary frequencies were obtained, the existence of this modification seems plausible.

Na_4SnSe_4. DFT calculations reveal Na_4SnSe_4-*tI*216 to be metastable as it is 2.5 kJ mol^{-1} higher in energy relative to that of Na_4SnSe_4-*tP*18.

In contrast to Na_4SiSe_4, for Na_4SnSe_4 both experimentally observed modifications are lower in energy than all of the other investigated structure types. Na_4SnSe_4-*tI*216 is 2.5 kJ mol^{-1} higher in energy relative to Na_4SnSe_4-*tP*18. Na_4SnSe_4 in the Na_4GeSe_4 structure type is 24.1 kJ mol^{-1} higher in energy. Na_4SnSe_4-*oP*36 (K_4SnSe_4 structure type) and Na_4SnSe_4-*cP*72 (Ba_4SiAs_4 structure type) are 29.6 and 37.7 kJ mol^{-1} higher in energy, respectively. The existence of further modifications of Na_4SnSe_4 in the other mentioned structure types seems implausible.

Band Structures. Electronic band structures of all title compounds were calculated within the DFT framework using hybrid HSE06 and are shown in the Supporting Information (Figure S11). Na_4SiSe_4-*oP*36 and Na_4SiSe_4-*cP*72 show direct band gaps of 4.01 and 4.28 eV, respectively. Na_4GeSe_4 exhibits an indirect band gap of 3.25 eV. Na_4SnSe_4-*tP*18 shows a direct band gap of 2.75 eV, whereas Na_4SnSe_4-*tI*216 has a direct band gap of 2.50 eV. Experiments reveal two band gaps for Na_4SnSe_4-*tP*18 where the larger one corresponds to the calculated value (2.86 eV).[60] The band gap decreases on going from Si to the higher homologues Ge and Sn. This is also in line with the observed colors of the synthesized powder samples and matches the chemical expectation. Powder samples of both modifications of Na_4SiSe_4 are light brown to white, Na_4GeSe_4 appears light yellow, and both modifications of Na_4SnSe_4 look yellow to orange.

https://doi.org/10.1021/acs.chemmater.4c00670
Chem. Mater. 2024, 36, 5643−5650

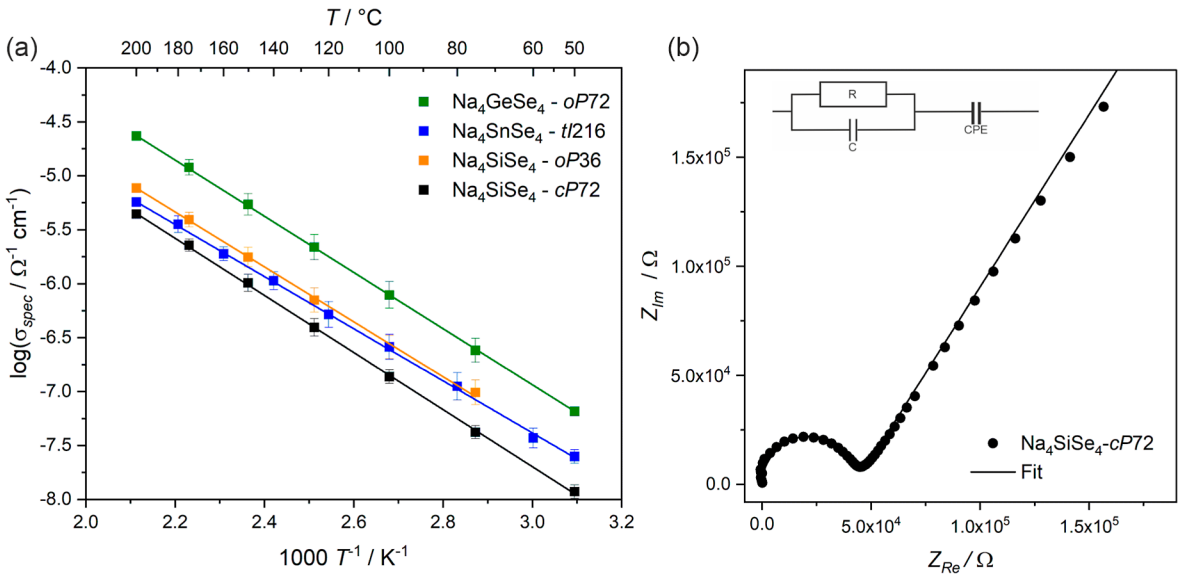

Figure 6. (a) Temperature-dependent specific ionic conductivity of Na_4SiSe_4-*oP*36, Na_4SiSe_4-*cP*72, and Na_4SnSe_4-*tI*216 with linear fit (solid line). (b) Nyquist plot for Na_4SiSe_4-*cP*72 at 200 °C with fit.

Impedance Spectroscopy. Samples of Na_4SiSe_4-*cP*72, Na_4SiSe_4-*oP*36, Na_4GeSe_4 and Na_4SnSe_4-*tI*216 were analyzed by impedance spectroscopy to check for Na ion conductivity. The size of the band gaps (DFT calculations and color of the samples) indicates that the measured conductivities are predominantly based on ion transport. This is also in line with the Nyquist plots and fitted impedance spectra (Figure 6).

Na_4GeSe_4-*oP*72 shows the highest conductivity with σ_{spec} = 6.6×10^{-8} Ω^{-1} cm^{-1} at 50 °C and σ_{spec} = 2.4×10^{-5} Ω^{-1} cm^{-1} at 200 °C. The activation energy of 0.52 eV was extracted from the Arrhenius plot of the fitted impedance data at different temperatures (Figure 6a). The other examined compounds showed slightly lower ionic conductivities. The temperature-dependent specific ionic conductivities of all compounds are shown in Figure 6a. As there is no deviation from the linear behavior, phase transitions during the measurement can be excluded. In Figure 6b, a representative Nyquist plot of Na_4SiSe_4-*cP*72 is shown. Further Nyquist plots can be found in the Supporting Information (Figure S14). Selected ionic conductivities and activation energies of all compounds are listed in Table 3. It has to be taken into account that conductivity measurements differing by less than 1 order of magnitude are not significantly different. Despite structural differences of the investigated materials, there is no obvious rule to explain the trend in ionic conductivities of Na_4TtSe_4. A clear influence of the Na coordination on the ion conductivity is not visible. Generally speaking, a higher versatility in the Na coordination environment and the resulting flatter energy surface should enhance Na ion migration.[30] In comparison to the other investigated materials, the Na coordination environment in Na_4SiSe_4-*cP*72 is the least distorted. This corresponds to the lowest ion conductivity.

Other selenotetrelates like Na_4SnSe_4-*tP*18 and $Na_4Si_2Se_6$-*oP*48 show similar ionic conductivities (σ_{spec} = 1.13×10^{-8} Ω^{-1} cm^{-1} at 20 °C[32] and σ_{spec} = 1.4×10^{-8} Ω^{-1} cm^{-1} at 50 °C[29]).

Table 3. Selected Ionic Conductivites and Activation Energies for Na_4SiSe_4-*oP*36, Na_4SiSe_4-*cP*72, Na_4GeSe_4-*oP*72, and Na_4SnSe_4-*tI*216 Determined by Impedance Spectroscopy

compound	σ_{spec}(50°C)/Ω^{-1} cm^{-1}	σ_{spec}(200°C)/Ω^{-1} cm^{-1}	E_a/eV
Na_4SiSe_4-*oP*36	1.0×10^{-7}[a]	7.7×10^{-6}	0.41
Na_4SiSe_4-*cP*72	1.1×10^{-8}	4.4×10^{-6}	0.53
Na_4GeSe_4-*oP*72	6.6×10^{-8}	2.4×10^{-5}	0.52
Na_4SnSe_4-*tI*216	2.5×10^{-8}	5.7×10^{-6}	0.47

[a]At 75 °C.

CONCLUSIONS

Sodium selenotetrelate compounds Na_4TtSe_4 (*Tt* = Si, Ge, Sn) were synthesized by two-step solid-state reactions. The preparation of two new compounds was possible via a two-step synthesis procedure consisting of mechanochemical homogenization of the elements, followed by annealing of the reaction mixture. The new modification of Na_4SiSe_4, Na_4SiSe_4-*cP*72, crystallizes in the cubic space group $P\bar{4}3n$ (no. 218) in the Ba_4SiAs_4 structure type and has a calculated band gap of 4.28 eV. The formation of both modifications from the ball-milled reaction mixture was investigated by in situ high-temperature X-ray powder diffraction. According to Ostwald's rule, at first a metastable modification, Na_4SiSe_4-*oP*36, is formed. By heating further, Na_4SiSe_4-*cP*72 is observed, which is stable up to 400 °C. At even higher temperatures, the cubic modification retransforms to Na_4SiSe_4-*oP*36. DFT calculations confirm Na_4SiSe_4-*cP*72 to be the more stable modification (ΔE = 8.6 kJ mol^{-1}). DFT modeling of further hypothetical structure types for the 4:1:4 composition revealed only small energy differences. Hypothetical Na_4SiSe_4-*tP*18 (Na_4SnS_4 structure type) is 1.9 kJ mol^{-1} lower in energy than Na_4SiSe_4-*cP*72, which was experimentally observed. Phonon dispersion calculations for Na_4SiSe_4-*tP*18 showed no imaginary frequencies. Therefore, the existence of this compound seems conceivable.

Also for Na_4SnSe_4, a new modification had been synthesized. The crystal structure was determined by single-crystal X-ray diffraction. Na_4SnSe_4-*tI*216 crystallizes in the tetragonal space group $I4_1/acd$ (no. 142) in the Na_4SnTe_4-*tI*216 structure type with a calculated band gap of 2.50 eV. DFT calculations reveal Na_4SnSe_4-*tI*216 to be metastable. The already known

https://doi.org/10.1021/acs.chemmater.4c00670
Chem. Mater. 2024, 36, 5643−5650

modification, Na_4SnSe_4-*tP*18, is more stable by 2.5 kJ mol^{-1}. The phase transition was not examined in detail.

Calculations of *E*−*V*-curves for Na_4GeSe_4 in different hypothetic structure types show that there are three different structure types that are lower in energy with respect to the experimentally observed Na_4GeSe_4-*oP*72. The existence of further modifications of Na_4GeSe_4 seems plausible. Phonon dispersion calculations for Na_4GeSe_4 in the Na_4SnS_4 structure type show no imaginary frequencies and, therefore, indicate dynamic stability.

Impedance spectroscopy measurements were performed for all of the title compounds. All materials showed moderate sodium ion conductivity. The best ion conductivity was determined for Na_4GeSe_4 ($\sigma_{spec} = 6.6 \times 10^{-8}$ S cm^{-1} at 50 °C).

■ ASSOCIATED CONTENT

Supporting Information

The Supporting Information is available free of charge at https://pubs.acs.org/doi/10.1021/acs.chemmater.4c00670.

Crystallographic data of Na_4SiSe_4 (CIF)

Crystallographic data of Na_4SnSe_4 (CIF)

Additional experimental and calculation details, including X-ray powder data, DTA measurements, and Nyquist plots of EIS measurements (PDF)

■ AUTHOR INFORMATION

Corresponding Authors

Florian Pielnhofer − *Institut für Anorganische Chemie, University of Regensburg, Regensburg 93053, Germany;* orcid.org/0000-0001-5309-4301; Email: florian.pielnhofer@ur.de

Arno Pfitzner − *Institut für Anorganische Chemie, University of Regensburg, Regensburg 93053, Germany;* orcid.org/0000-0001-8653-7439; Email: arno.pfitzner@ur.de

Author

Franziska Kamm − *Institut für Anorganische Chemie, University of Regensburg, Regensburg 93053, Germany*

Complete contact information is available at: https://pubs.acs.org/10.1021/acs.chemmater.4c00670

Notes

The authors declare no competing financial interest.

■ REFERENCES

(1) Janek, J.; Zeier, W. G. A solid future for battery development. *Nat. Energy* **2016**, *1*, 16141.

(2) Zhang, Z.; Shao, Y.; Lotsch, B.; Hu, Y.-S.; Li, H.; Janek, J.; Nazar, L. F.; Nan, C.-W.; Maier, J.; Armand, M.; et al. New horizons for inorganic solid state ion conductors. *Energy Environ. Sci.* **2018**, *11*, 1945−1976.

(3) Yabuuchi, N.; Kubota, K.; Dahbi, M.; Komaba, S. Research Development on Sodium-Ion Batteries. *Chem. Rev.* **2014**, *114*, 11636−11682.

(4) Kundu, D.; Talaie, E.; Duffort, V.; Nazar, L. F. The Emerging Chemistry of Sodium Ion Batteries for Electrochemical Energy Storage. *Angew. Chem., Int. Ed.* **2015**, *54*, 3431−3448.

(5) Delmas, C. Sodium and Sodium-Ion Batteries: 50 Years of Research. *Adv. Energy Mater.* **2018**, *8*, 1703137.

(6) Jansen, M.; Henseler, U. Synthesis, structure determination, and ionic conductivity of sodium tetrathiophosphate. *J. Solid State Chem.* **1992**, *99*, 110−119.

(7) Hayashi, A.; Noi, K.; Tanibata, N.; Nagao, M.; Tatsumisago, M. High sodium ion conductivity of glass−ceramic electrolytes with cubic Na_3PS_4. *J. Power Sources* **2014**, *258*, 420−423.

(8) Zhang, L.; Yang, K.; Mi, J.; Lu, L.; Zhao, L.; Wang, L.; Li, Y.; Zeng, H. Na_3PSe_4: A Novel Chalcogenide Solid Electrolyte with High Ionic Conductivity. *Adv. Energy Mater.* **2015**, *5*, 1501294.

(9) Krauskopf, T.; Pompe, C.; Kraft, M. A.; Zeier, W. G. Influence of Lattice Dynamics on Na^+ Transport in the Solid Electrolyte $Na_3PS_{4-x}Se_x$. *Chem. Mater.* **2017**, *29*, 8859−8869.

(10) Krauskopf, T.; Muy, S.; Culver, S. P.; Ohno, S.; Delaire, O.; Shao-Horn, Y.; Zeier, W. G. Comparing the Descriptors for Investigating the Influence of Lattice Dynamics on Ionic Transport Using the Superionic Conductor $Na_3PS_{4-x}Se_x$. *J. Am. Chem. Soc.* **2018**, *140*, 14464−14473.

(11) Richards, W. D.; Tsujimura, T.; Miara, L. J.; Wang, Y.; Kim, J. C.; Ong, S. P.; Uechi, I.; Suzuki, N.; Ceder, G. Design and synthesis of the superionic conductor $Na_{10}SnP_2S_{12}$. *Nat. Commun.* **2016**, *7*, 11009.

(12) Duchardt, M.; Ruschewitz, U.; Adams, S.; Dehnen, S.; Roling, B. Vacancy-Controlled Na^+ Superion Conduction in $Na_{11}Sn_2PS_{12}$. *Angew. Chem., Int. Ed.* **2018**, *57*, 1351−1355.

(13) Tanibata, N.; Noi, K.; Hayashi, A.; Tatsumisago, M. Preparation and characterization of highly sodium ion conducting Na_3PS_4−Na_4SiS_4 solid electrolytes. *RSC Adv.* **2014**, *4*, 17120−17123.

(14) Kaib, T.; Bron, P.; Haddadpour, S.; Mayrhofer, L.; Pastewka, L.; Järvi, T. T.; Moseler, M.; Roling, B.; Dehnen, S. Lithium Chalcogenidotetrelates: LiChT—Synthesis and Characterization of New Li^+ Ion Conducting Li/Sn/Se Compounds. *Chem. Mater.* **2013**, *25*, 2961−2969.

(15) Minafra, N.; Hogrefe, K.; Barbon, F.; Helm, B.; Li, C.; Wilkening, H. M. R.; Zeier, W. G. Two-Dimensional Substitution: Toward a Better Understanding of the Structure−Transport Correlations in the Li-Superionic Thio-LISICONs. *Chem. Mater.* **2021**, *33*, 727−740.

(16) Klepp, K. O. Darstellung und Kristallstruktur von Na_4GeSe_4: ein neues ortho-Selenogermanat(IV). *Z. Naturforsch., B: J. Chem. Sci.* **1985**, *40*, 878−882.

(17) Klepp, K. O. Na_4SnSe_4 und K_4SnSe_4, zwei neue Selenostannate mit isolierten Anionen/Na_4SnSe_4 and K_4SnSe_4, Two New Selenostannates with Discrete Anions. *Z. Naturforsch., B: J. Chem. Sci.* **1992**, *47*, 411−417.

(18) Preishuber-Pflügl, H.; Klepp, K. O. Crystal structure of tetrasodium tetraselenidosilicate(IV). Na_4SiSe_4. *Z. Kristallogr.—New Cryst. Struct.* **2003**, *218*, 415.

(19) Eisenmann, B.; Jordan, H.; Schäfer, H. Zintlphasen mit isolierten $SiAs_4$- bzw. $GeAs_4$-Anionen: Darstellung und Struktur von Ba_4SiAs_4 und Ba_4GeAs_4 sowie Sr_4SiAs_4 und Sr_4GeAs_4. *Z. Anorg. Allg. Chem.* **1981**, *475*, 74−80.

(20) Schlirf, J.; Deiseroth, H. J.; Nilges, T. Crystal structure of cesium ortho-selenosilicate. Cs_4SiSe_4. *Z. Kristallogr.—New Cryst. Struct.* **2000**, *215*, 343−344.

(21) Eisenmann, B.; Hansa, J. Crystal structure of hexasodium heptaselenodisilicate, $Na_6Si_2Se_7$. *Z. Kristallogr.—Cryst. Mater.* **1993**, *203*, 295−296.

(22) Eisenmann, B.; Hansa, J.; Schäfer, H. Zur Kenntnis der Selenidosilikate und -germanate $Na_4Si_4Se_{10}$, Na_2GeSe_3 und $Na_8Ge_4Se_{10}$. *Z. Naturforsch., B: J. Chem. Sci.* **1985**, *40*, 450−457.

(23) Eisenmann, B.; Hansa, J.; Schäfer, H. $Na_2Ge_2Se_5$, das erste Schichtselenidogermanat. *Rev. Chim. Minér.* **1984**, *21*, 817−823.

(24) Eisenmann, B.; Hansa, J.; Schäfer, H. $Na_6Si_2Se_8$: Ein Perselenidosilicat. *Z. Anorg. Allg. Chem.* **1985**, *526*, 55−59.

(25) Eisenmann, B.; Hansa, J. Crystal structure of tetrasodium decaselenotetragermanate, $Na_4[Ge_4Se_{10}]$. *Z. Kristallogr.—Cryst. Mater.* **1993**, *205*, 325−326.

(26) Eisenmann, B.; Hansa, J.; Schäfer, H. Oligoselenidogermanate (III): Zur Kenntnis von $Na_6Ge_2Se_6$ und $Na_8Ge_4Se_{10}$. *Mater. Res. Bull.* **1985**, *20*, 1339−1346.

(27) Eisenmann, B.; Kieselbach, E.; Schäfer, H.; Schrod, H. On Thiogermanates, Selenidogermanates, and Telluridogermanates

(III)—$K_6Ge_2S_6$, $K_6Ge_2Se_6$, and $Na_6Ge_2Te_6$. *Z. Anorg. Allg. Chem.* **1984**, *516*, 49−54.
(28) Eisenmann, B.; Schwerer, H.; Schäfer, H. $Na_6Si_2Te_6$—ein neues Tellurohypodisilikat/$Na_6Si_2Te_6$—A New Tellurohypodisilicate. *Z. Naturforsch. B* **1981**, *36*, 1538−1541.
(29) Kamm, F.; Pielnhofer, F.; Schlosser, M.; Pfitzner, A. Synthesis and Characterization of $Na_4Si_2Se_6$-tP24 and $Na_4Si_2Se_6$-oP48, Two Polymorphs with Different Anionic Structures. *Inorg. Chem.* **2023**, *62*, 11064−11072.
(30) Harm, S.; Hatz, A.-K.; Schneider, C.; Hoefer, C.; Hoch, C.; Lotsch, B. V. Finding the Right Blend: Interplay Between Structure and Sodium Ion Conductivity in the System Na_5AlS_4−Na_4SiS_4. *Front. Chem.* **2020**, *8*, 90.
(31) Ben Yahia, H.; Motohashi, K.; Mori, S.; Sakuda, A.; Hayashi, A. Synthesis, structure and properties of Na_4GeS_4. *J. Alloys Compd.* **2023**, *960*, 170600.
(32) Gao, L.; Bian, G.; Yang, Y.; Zhang, B.; Wu, X.; Wu, K. Na_4SnS_4 and Na_4SnSe_4 exhibiting multifunctional physicochemical performances as potential infrared nonlinear optical crystals and sodium ion conductors. *New J. Chem.* **2021**, *45*, 12362−12366.
(33) Hartmann, F.; Benkada, A.; Indris, S.; Poschmann, M.; Lühmann, H.; Duchstein, P.; Zahn, D.; Bensch, W. Directed Dehydration as Synthetic Tool for Generation of a New Na_4SnS_4 Polymorph: Crystal Structure, Na^+ Conductivity, and Influence of Sb-Substitution. *Angew. Chem., Int. Ed.* **2022**, *61*, No. e202202182.
(34) Matsushita, Y.; Kanatzidis, M. G. Synthesis and Structure of Li_4GeS_4. *Z. Naturforsch. B* **1998**, *53*, 23−30.
(35) Jumas, J.-C.; Philippot, E.; Vermot-Gaud-Daniel, F.; Ribes, M.; Maurin, M. Etude de la tétracoordination de l'etain dans deux orthothiostannates: Na_4SnS_4 et Ba_2SnS_4 (α). *J. Solid State Chem.* **1975**, *14*, 319−327.
(36) Melullis, M.; Dehnen, S. Syntheses, Crystal Structures, UV-Vis Spectra and First NMR Spectra of New Potassium Salts of Chalcogenogermanates. *Z. Anorg. Allg. Chem.* **2007**, *633*, 2159−2167.
(37) *STOE WinXPow*; Stoe & Cie GmbH: Darmstadt, Germany, 2016.
(38) Petříček, V.; Dušek, M.; Palatinus, L. Crystallographic Computing System JANA2006: General features. *Z. Kristallogr.—Cryst. Mater.* **2014**, *229*, 345−352.
(39) Palatinus, L.; Chapuis, G. SUPERFLIP − a computer program for the solution of crystal structures by charge flipping in arbitrary dimensions. *J. Appl. Crystallogr.* **2007**, *40*, 786−790.
(40) *CrysAlisPro (V42)*; Rigaku Oxford Diffraction Ltd, 2019.
(41) *Zahner-Elektrik Zahner Analysis. I*; Zahner-Schiller GmbH & Co. KG: Kronach, 2023.
(42) Dovesi, R.; Erba, A.; Orlando, R.; Zicovich-Wilson, C. M.; Civalleri, B.; Maschio, L.; Rérat, M.; Casassa, S.; Baima, J.; Salustro, S.; et al. Quantum-mechanical condensed matter simulations with CRYSTAL. *Wiley Interdiscip. Rev.: Comput. Mol. Sci.* **2018**, *8*, No. e1360.
(43) Dovesi, R.; Saunders, V. R.; Roetti, C.; Orlando, R.; Zicovich-Wilson, C. M.; Pascale, F.; Civalleri, B.; Doll, K.; Harrison, N. M.; Bush, I. J.; et al. *CRYSTAL17 User's Manual*; University of Torino, 2017.
(44) Sophia, G.; Baranek, P.; Sarrazin, C.; Rerat, M.; Dovesi, R. 2014. https://www.crystal.unito.it/Basis_Sets/sodium.html (accessed 03 06, 2023).
(45) Porter, A. R.; Towler, M. D.; Needs, R. J. Muonium as a hydrogen analogue in silicon and germanium: Quantum effects and hyperfine parameters. *Phys. Rev. B* **1999**, *60*, 13534−13546.
(46) Heyd, J.; Peralta, J. E.; Scuseria, G. E.; Martin, R. L. Energy band gaps and lattice parameters evaluated with the Heyd-Scuseria-Ernzerhof screened hybrid functional. *J. Chem. Phys.* **2005**, *123*, 174101.
(47) Causà, M.; Dovesi, R.; Roetti, C. Pseudopotential Hartree-Fock study of seventeen III-V and IV-IV semiconductors. *Phys. Rev. B* **1991**, *43*, 11937−11943.
(48) Towler, M. D.; Zicovich-Wilson, C. 1995. https://vallico.net/mike_towler/crystal.html (accessed 03 06, 2023).
(49) Becke, A. D. Density-functional exchange-energy approximation with correct asymptotic behavior. *Phys. Rev. A* **1988**, *38*, 3098−3100.
(50) Heyd, J.; Scuseria, G. E.; Ernzerhof, M. Hybrid functionals based on a screened Coulomb potential. *J. Chem. Phys.* **2003**, *118*, 8207−8215.
(51) Perdew, J. P.; Burke, K.; Ernzerhof, M. Generalized Gradient Approximation Made Simple. *Phys. Rev. Lett.* **1996**, *77*, 3865−3868.
(52) Murnaghan, F. D. Finite Deformations of an Elastic Solid. *Am. J. Math.* **1937**, *59*, 235−260.
(53) Murnaghan, F. D. The Compressibility of Media under Extreme Pressures. *Proc. Natl. Acad. Sci. U.S.A.* **1944**, *30*, 244−247.
(54) Birch, F. Finite Elastic Strain of Cubic Crystals. *Phys. Rev.* **1947**, *71*, 809−824.
(55) Hinuma, Y.; Pizzi, G.; Kumagai, Y.; Oba, F.; Tanaka, I. Band structure diagram paths based on crystallography. *Comput. Mater. Sci.* **2017**, *128*, 140−184.
(56) Pascale, F.; Zicovich-Wilson, C. M.; López Gejo, F.; Civalleri, B.; Orlando, R.; Dovesi, R. The calculation of the vibrational frequencies of crystalline compounds and its implementation in the CRYSTAL code. *J. Comput. Chem.* **2004**, *25*, 888−897.
(57) Zicovich-Wilson, C. M.; Pascale, F.; Roetti, C.; Saunders, V. R.; Orlando, R.; Dovesi, R. Calculation of the vibration frequencies of α-quartz: The effect of Hamiltonian and basis set. *J. Comput. Chem.* **2004**, *25*, 1873−1881.
(58) Föppl, H.; Busmann, E.; Frorath, F.-K. Die Kristallstrukturen von α-Na_2S_2 und K_2S_2, β-Na_2S_2 und Na_2Se_2. *Z. Anorg. Allg. Chem.* **1962**, *314*, 12−20.
(59) Zagler, R. Darstellung und Strukturchemie von Chalkogenido-Polyanionen und Chalkogenidoindaten, -germanaten, -stannaten, -arsenaten, -antimonaten bzw. -telluraten mit komplexierten und nicht komplexierten Kationen. Ph.D. Thesis, Universität Darmstadt, 1988.
(60) Palchik, O.; Gedanken, A.; Palchik, V.; Slifkin, M.; Weiss, A. Microwave-Assisted Preparation, Morphological, and Photoacoustic Studies of the Na_4SnSe_4, $K_4Sn_2Se_6$, and $K_4Sn_3Se_8$, Zintl Molecular Sn−Se Oligomers. *J. Solid State Chem.* **2002**, *165*, 125−130.

https://doi.org/10.1021/acs.chemmater.4c00670
Chem. Mater. 2024, 36, 5643−5650